

RESEARCH ARTICLE

Biom mineralization-related specialization of hemocytes and mantle tissues of the Pacific oyster *Crassostrea gigas*

Anna V. Ivanina^{1,*}, Halina I. Falfushynska^{2,*}, Elia Beniash³, Helen Piontkivska⁴ and Inna M. Sokolova^{5,‡}

ABSTRACT

The molluscan exoskeleton (shell) plays multiple important roles including structural support, protection from predators and stressors, and physiological homeostasis. Shell formation is a tightly regulated biological process that allows molluscs to build their shells even in environments unfavorable for mineral precipitation. Outer mantle edge epithelial cells (OME) and hemocytes were implicated in this process; however, the exact functions of these cell types in biomineralization are not clear. Pacific oysters (*Crassostrea gigas*) were used to study differences in the expression profiles of selected biomineralization-related genes in hemocytes and mantle cells, and the functional characteristics of hemocytes such as adhesion, motility and phagocytosis. The specialized role of OME in shell formation was supported by high expression levels of the extracellular matrix (ECM) related and cell–cell interaction genes. Density gradient separation of hemocytes revealed distinct phenotypes based on the cell morphology, gene expression patterns, motility and adhesion characteristics. These hemocyte fractions can be categorized into two functional groups, i.e. biomineralization and immune response cells. Gene expression profiles of the putative biomineralizing hemocytes indicate that in addition to their proposed role in mineral transport, hemocytes also contribute to the formation of the ECM, thus challenging the current paradigm of the mantle as the sole source of the ECM for shell formation. Our findings corroborate the specialized roles of hemocytes and the OME in biomineralization and emphasize complexity of the biological controls over shell formation in bivalves.

KEY WORDS: Gene expression, Ion transport, Matrix protein, Exoskeleton, Cell–cell interaction, Immunity, Bivalve

INTRODUCTION

Molluscs are the second most abundant and species-rich group of invertebrates with a high degree of morphological and ecological diversity (Kocot et al., 2016). Molluscs are found in marine, freshwater and terrestrial habitats, and are dominant species and ecosystem engineers in many biotopes (Gutiérrez et al., 2003). The ecological and evolutionary success of molluscs is at least in part attributed to their exoskeleton (shell), which provides structural


support, protection from predators and stressors, and contributes to physiological homeostasis (Crenshaw, 1972; Sokolova et al., 2000; Furuhashi et al., 2009; Haszprunar and Wanninger, 2012). Molluscan shells are complex mineral-organic composites that possess unique structural organization and mechanical properties superior to geological calcium carbonates (Smith et al., 1999; Kamat et al., 2000; Marin and Luquet, 2004). Shell formation is a tightly regulated biological process that allows molluscs to build and maintain their shells in different environments, including those unfavorable for mineral precipitation (Ries et al., 2009; Beniash et al., 2010; Dickinson et al., 2012, 2013). Due to the complexity of molluscan biomineralization, this process is not yet fully understood despite decades of investigations (Addadi et al., 2006; Furuhashi et al., 2009). Recent advances in molecular and cell biology provide new tools for resolving long-standing questions about molluscan biomineralization that can shed light on the regulation of the complex process of shell formation.

Molluscan shells consist of periostracum (the outermost proteinaceous layer covering the shell) as well as the middle (ostracum) and inner (hypostracum) layers made of highly organized calcium carbonate (CaCO₃) crystals with less than 5% w/w of organic material (Zhang and Zhang, 2006; Furuhashi et al., 2009). The outer mantle edge (OME) has been traditionally associated with biomineralization due to its proximity to the shell surface and ability to maintain shell deposition *ex vivo*, albeit at a reduced rate (Jodrey, 1953; Wilbur and Jodrey, 1955). Recent studies in mantle transcriptomics and proteomics revealed staggering diversity of the protein ensemble expressed in the mantle and involved in shell formation (Jackson et al., 2006; Zhang and Zhang, 2006; Marin et al., 2008; Jackson et al., 2010; Gardner et al., 2011; Kocot et al., 2016; Li et al., 2016). Mantle cells produce the components of the shell organic extracellular matrix (ECM) traditionally divided into two major fractions: insoluble proteins (primarily chitin and silk) that act as a scaffold for crystal growth and play a role in the mechanical reinforcement of the shells, and soluble proteins and proteoglycans involved in the regulation of mineral nucleation and growth (Weiner et al., 1984; Falini et al., 1996; Mayer and Sarikaya, 2002; Addadi et al., 2006; Marin et al., 2008; Marie et al., 2012). These molecules function as Ca²⁺ chelators, mineralization nucleators or inhibitors (Nudelman et al., 2006), regulate crystal shape (Albeck et al., 1993), determine which CaCO₃ polymorph will form (Falini et al., 1996; Marie et al., 2012), and may play a role in toughening of the shells (Smith et al., 1999). Although the organic fraction of the shell is small, it is critically important for regulation of the shell formation, structure and mechanical properties (Addadi et al., 2006; Zhang and Zhang, 2006; Marin et al., 2008; Kocot et al., 2016). Whilst the important role of the mantle in biomineralization is undisputed, there is increasing evidence for involvement of other cell types, notably hemocytes in biomineralization (Fisher, 2004; Mount et al., 2004; Johnstone et al., 2015). Studies suggest that hemocytes sequester

¹Department of Biological Sciences, University of North Carolina at Charlotte, Charlotte, NC 28223, USA. ²Department of Human Health, I.Ya. Horbachevsky Ternopil State Medical University, Ternopil 46000, Ukraine. ³Department of Oral Biology, School of Dental Medicine, University of Pittsburgh, Pittsburgh, PA 15261, USA. ⁴Department of Biological Sciences, Kent State University, Kent, OH 44240, USA. ⁵Department of Marine Biology, Institute of Biosciences, University of Rostock, Rostock 18059, Germany.

*These authors contributed equally to this work

‡Author for correspondence (Inna.Sokolova@uni-rostock.de)

 H.I.F., 0000-0003-3058-4919; I.M.S., 0000-0002-2068-4302

List of abbreviations

ASW	artificial seawater
CA	carbonic anhydrase
ECM	extracellular matrix
OME	outer mantle edge
SLP	silk-like protein
VEGF	vascular endothelial growth factor
VEGF-R	vascular endothelial growth factor receptor

Ca^{2+} and CO_3^{2-} and transport them intracellularly in a form of calcium carbonate mineral to the shell mineralization sites (Mount et al., 2004; Johnstone et al., 2008, 2015). This is a paradigm-shifting observation in molluscan biomineralization, albeit the important role of cellular mineral transport has been shown in echinoderms and vertebrates (Beniash et al., 1999; Mahamid et al., 2011; Boonrungsiman et al., 2012; Vidavsky et al., 2014; Akiva et al., 2015; Vidavsky et al., 2015). To date, the interactions between different types of biomineralizing cells of molluscs, including mantle cells and hemocytes, and their potential specialization with regard to key biomineralization processes (such as acid–base and ion regulation, mineral transport, and production of regulatory and matrix proteins) are not well understood and require further investigation.

We used Pacific oysters, *Crassostrea gigas*, as a model to study specialization of molecular pathways involved in biomineralization between different molluscan cell types (hemocytes and mantle cells). Oysters are an excellent model to study biomineralization mechanisms due to extensive information on their shell mineral composition, structure and mechanical properties (Choi and Kim, 2000; Checa et al., 2007; Lee et al., 2008; Beniash et al., 2010; Dickinson et al., 2012; Dauphin et al., 2013) and availability of the annotated genome (Zhang et al., 2012) permitting targeted analysis of biomineralization-related genes. In this study, we hypothesized that hemocytes and mantle cells play distinct roles in shell biomineralization, with hemocytes primarily responsible for the mineral sequestration and delivery, and the mantle cells involved in the ECM deposition and regulation of the physicochemical conditions at the mineralization site. We also hypothesized that ECM production predominantly occurs in the OME, while the central part of the mantle contributes to the acid–base and ion regulation of the pallium, including the mineralization site. To test these hypotheses, we investigated Ca^{2+} content, cellular adhesion and motility of different subpopulations of oyster hemocytes, and studied mRNA expression of biomineralization-related genes in hemocytes and mantle cells from the central and outer edge mantle of *C. gigas*. We focused on the key genes involved in production and maturation of the matrix proteins [including silk-like protein (SLP), nacrein, chitin synthases and casein kinases], cell–cell and cell–matrix interactions (fibronectin and fibronectin-ankyrin), and acid–base and ion regulation (including different isoforms of carbonic anhydrase, V-type H^+ -ATPase, Na^+/H^+ -antiprotectors and Ca^{2+} -ATPases). We also investigated mRNA expression of the vascular endothelial growth factor (VEGF) and its receptor (VEGF-R) that are involved in regulation of crystal formation and growth in marine organisms such as echinoderms (Duloquin et al., 2007; Knapp et al., 2012). Gills were used as a reference non-biomineralizing tissue. Our data provide insights into the specialization of hemocytes and mantle cells on different biomineralization-related functions and shed light on the role of hemocyte diversity in molluscan biomineralization.

MATERIALS AND METHODS**Animals**

Oysters *Crassostrea gigas* (Thunberg 1793) from Fanny Bay (British Columbia, Canada) were purchased from a local supplier (Inland Seafood, Charlotte, NC, USA). Oysters were kept in tanks filled with artificial seawater (ASW) (Instant Ocean, Kent Marine, Acworth) at $10 \pm 1^\circ\text{C}$ and salinity 30 ± 1 practical salinity units (PSU) and fed *ad libitum* with a commercial algal blend containing *Nannochloropsis oculata*, *Phaeodactylum tricornutum* and *Chlorella* spp. (DT's Live Marine Phytoplankton, Sycamore, IL, USA). Algal blend (2–3 ml per 20–25 animals) was added to experimental tanks every other day.

Hemolymph collection and hemocyte fractionation

Hemolymph was withdrawn from the adductor muscle of oysters using a syringe containing 1 ml cold Alsever's solution [20.8 g l^{-1} glucose, 8 g l^{-1} sodium citrate, 3.36 g l^{-1} ethylenediaminetetraacetic acid (EDTA), 22.3 g l^{-1} NaCl]. To obtain sufficient number of hemocytes, hemolymph from 7–15 animals was pooled. Separate samples of pooled hemolymph obtained from different oysters were considered biological replicates. Hemolymph was centrifuged at 1000 g and $+4^\circ\text{C}$ for 10 min. Pellets were resuspended in 4 ml Alsever's solution and layered on a discontinuous gradient of Percoll (9.2, 24.8, 41.0 and 57.8% v/v). Cells were centrifuged at 600 g and $+4^\circ\text{C}$ for 40 min. Hemocytes concentrated at different interfaces of the discontinuous gradient were collected separately, diluted 10- to 12-fold with Alsever's solution and centrifuged at 1000 g for 10 min to remove Percoll. Four subpopulations of hemocytes were separated using this method and labelled H1, H2, H3 and H4 (from the lowest to the highest floating density). The hemocyte pellets were resuspended in Alsever's solution and either used immediately for functional studies, or frozen at -80°C for subsequent gene expression analyses.

Cell morphology

Suspensions ($100 \mu\text{l}$) of different hemocyte fractions were placed on microscope slides, air dried and stained to access the morphology. For hematoxylin-eosin staining, hemocytes were fixed for 15 min in 10% formaldehyde, followed by stepwise rehydration in 100, 90 and 70% ethanol. Slides were stained in hematoxylin for 5 min, rinsed with water and differentiated in 1% acid alcohol for 5 min. Slides were again rinsed in water and stained with 1% eosin for 10 min followed by a stepwise dehydration (70, 90 and 100% ethanol). For Wright–Giemsa stain, air-dried hemocytes were immersed in Wright–Giemsa dye for 30 s, rinsed with water and air dried. Separate aliquots of hemocytes suspension were stained with Neutral Red to differentiate between acid (stained red) and basic (stained yellow) vesicles (Lowe and Pipe, 1994). Stock was prepared by dissolving 20 mg of Neutral Red in 1 ml dimethyl sulfoxide (DMSO), gravity-filtered and diluted 1:5 with phosphate-buffered saline (Lowe and Pipe, 1994). Slides with air-dried cells were stained with diluted Neutral Red solution for 5 min. All slides were rinsed with water and air dried prior to mounting in glycerol. Cells were observed under a Zeiss Axio Observer A1 inverted microscope equipped with an AxioCam HRC digital camera (Carl Zeiss, Oberkochen, Germany) using differential interference contrast illumination and a 63×1.4 numerical aperture plan apochromatic objective.

RNA isolation and real-time polymerase chain reaction

Total RNA was isolated from different fractions of hemocytes, the OME, the central part of the mantle, and the gills using TRI Reagent (Sigma-Aldrich, St Louis, MO, USA) according to the

manufacturer's instructions. To test for possible DNA contamination that could interfere with qRT-PCR, RNA samples were subjected to a PCR reaction with gene-specific primers (Table 1) prior to cDNA synthesis; no amplification product was observed, indicating no DNA contamination. Single-strand cDNA was then obtained from 1 µg of the total RNA using 50 U µl⁻¹ SMARTScribe Reverse Transcriptase (Clontech, Mountain View, CA, USA) and 20 µmol l⁻¹ of oligo (dT)₁₈ primers according to the manufacturer's instructions. Transcript levels of the genes of interest (including β-actin used as a reference gene) were quantified by RT-PCR using a 7500 Fast Real-Time PCR System (Life Technology, Carlsbad, CA, USA) and SYBR Green PCR kit (Life Technologies, Bedford, MA, USA) using gene-specific primers (Table 1). Annealing temperature was 55°C, and read temperature was 72°C

for all primer pairs. A single cDNA sample was used as an internal cDNA standard and included in each run to test for run-to-run amplification variability. Serial dilutions of the internal standard were amplified to determine apparent amplification efficiency (Pfaffl, 2001). Relative mRNA quantities of the target and reference genes were calculated according to Pfaffl (2001) using gene-specific amplification efficiencies.

Flow cytometry

To measure intracellular Ca²⁺ concentration ([Ca²⁺]_i), isolated hemocytes (10⁶ cells) were incubated for 30 min in ASW buffer with 1 µmol l⁻¹ calcein-AM (Invitrogen, Eugene, OR, USA). Following incubation, cells were washed and resuspended in 500 µl of ASW for analysis. To measure phagocytic activity, isolated

Table 1. Primer sequences for target genes in *Crassostrea gigas*

Target	Accession no.	Primer sequence
CA I	XM_011439428.2, LOC105335517	FW 5'-AGGGTTGATTCACTCCACATAC-3' Rev 5'-GCTCCATGGGATAAGAGATTCC-3'
CA II	XM_011449596.2, LOC105342594	FW 5'-CATCAACCAGCAGTCAGAAAGTA-3' Rev 5'-TGTTCCGATCCCTTGTCATTAG-3'
CA III	XM_011413668.2, LOC105317122	FW 5'-CTACCTACAACAGGGAGTTCTA-3' Rev 5'-CTGGTCTGAAATTGCCGTATCT-3'
CA VII	XM_011441430.2, LOC105336933	FW 5'-GCGGGAATGTAAGGGAGAAA-3' Rev 5'-GCATTGCTCTCCATGGTTATTG-3'
CA XIV	XM_011437076.2, LOC105336933	FW 5'-AGTGTTCAGGAGACCATCAAG-3' Rev 5'-CTGTGGTTGAGAGGCTGAATAG-3'
V-type H ⁺ -ATPase	XM_011420050.1, LOC105321678	FW 5'-GCAGTGTGAGCATTGTAGGA-3' Rev 5'-GTAGGAGATGAGCCAGTTGATG-3'
Ca ²⁺ -ATPase	XM_011430632.2, LOC105329397	FW 5'-AGGCAAAGGCATCGTCATAG-3' Rev 5'-GATGAGCCCCGATGATACAGAAG-3'
PM Ca ²⁺ -ATPase	XM_020071055.1, LOC105337328	FW 5'-CAACAAGGTCGCCAACAAAG-3' Rev 5'-GGTCAGTTTGCCCTGTAGAA-3'
NHX9	XM_011426556.2, LOC105326487	FW 5'-TGGTGAAGCTGACTGGTATTG-3' Rev 5'-CAATGGTTGCCGTCACAAAG-3'
NHE3	XM_011458684.2, LOC105349034	FW 5'-GATGATCCAGAGGAGAGCAAAG-3' Rev 5'-TTGTACGAGGGCTTTCTGTTAG-3'
Fibronectin Prot3L	XM_011437620.2, LOC105334248	FW 5'-CCAGGAGGAAATTTGAGGAGAG-3' Rev 5'-GTAATCATAGGGCACTGGTTTAG-3'
Fibronectin Prot2L	XM_011415804.1, LOC105318603	FW 5'-CTCCAGTACACCACAAGTCATC-3' Rev 5'-AGACACAACCTCCGGCAATATC-3'
Fibronectin ankyrin	XM_011451949.2, LOC105344232	FW 5'-CTAACAGTGTCCACCATAAGG-3' Rev 5'-CCTGTGTCCAGTATCCTCTCTA-3'
VEGF	XM_011451443.2, LOC105343926	FW 5'-CCGGTGCATGTGTACCAATA-3' Rev 5'-TGATTTCTCGTCAGTCATTCC-3'
VEGF-R	XM_011457891.1, LOC105348465	FW 5'-CGGCTATGGCTCTGCATAAA-3' Rev 5'-CAAATGCACCTTGACCCAATAC-3'
Casein kinase I	XM_011448074.2, LOC105341513	FW 5'-GGAGGTGGCTGTTAAGTTAGAG-3' Rev 5'-GCGAGCAGAAGTTGAAGAGA-3'
Casein kinase II	XM_011419091.2, LOC105320946	FW 5'-CGATGAAGCAGAGATCCCATA-3' Rev 5'-CAAACAGCACATGACCAACTAC-3'
Chitin synthase I	XM_020066933.1, LOC105327560	FW 5'-GAAGACACTGCTCGGTCATATT-3' Rev 5'-GGTGACTCAAAGTCCATTCT-3'
Chitin synthase II	XM_011425423.2, LOC105325734	FW 5'-CGCAACAATGGGCAATAGAG-3' Rev 5'-CTGATATCGAGGCGGTGAATAG-3'
Chitin synthase III	JH816899.1, CGI_10012656	FW 5'-GTACAAATGGGCTCTGGGATAG-3' Rev 5'-GTCGAACTCACACTGGAAGAA-3'
Nacrein	NM_001305309.1, LOC105335878	FW 5'-CGCCGAGAGAAACCTCTAAAT-3' Rev 5'-CCAGAGCCAAACTACGCTTAC-3'
SLP	AB290411.1	FW 5'-GATCTCCGCTTTACGTCCTATC-3' Rev 5'-AACCCGAGTAAGGTGTTGTATC-3'
β-actin	X75894	Act-FW 5'-TTGGACTTCGAGCAGGAGATGGC-3' Act-Rev 5'-ACATGGCCTCTGGGCACCTGA-3'

FW, forward; Rev, reverse; CA, carbonic anhydrase; Ca²⁺-ATPase, calcium-transporting ATPase type 2C; PM Ca²⁺-ATPase, plasma membrane calcium-transporting ATPase; fibronectin Prot2L and Prot3L, fibronectin type-III domain-containing protein 2 and 3a, respectively; VEGF, vascular endothelial growth factor; VEGF-R, vascular endothelial growth factor receptor; NHX9, sodium-proton antiporter NHX9; NHE3, sodium-proton exchanger 3; SLP, silk-like protein.

Table 2. ANOVA: effects of tissue type and/or hemocyte fraction on the expression of studied mRNAs in *Crassostrea gigas*

Gene	Factor effect	Gene	Factor effect
CA I	$F_{6,43}=10.4$ $P<0.001$	SLP	$F_{6,43}=71.7$ $P<0.001$
CA II	$F_{6,43}=10.3$ $P<0.001$	Fibronectin Prot2L	$F_{6,43}=27.4$ $P<0.001$
CA III	$F_{6,43}=22.5$ $P<0.001$	Fibronectin Prot3L	$F_{6,43}=9.6$ $P<0.001$
CA VII	$F_{6,43}=15.0$ $P<0.001$	Fibronectin ankyrin	$F_{6,43}=10.4$ $P<0.001$
CA XIV	$F_{6,43}=3.9$ $P=0.004$	Nacrein	$F_{6,43}=10.4$ $P<0.001$
V-type H ⁺ -ATPase	$F_{6,43}=3.6$ $P=0.005$	VEGF	$F_{6,43}=67.7$ $P<0.001$
Ca ²⁺ -ATPase	$F_{6,43}=6.6$ $P<0.001$	VEGF receptor	$F_{6,43}=3.5$ $P=0.006$
PM Ca ²⁺ -ATPase	$F_{6,43}=8.0$ $P<0.001$	Casein kinase I	$F_{6,43}=15.7$ $P<0.001$
NHX9	$F_{6,43}=8.6$ $P<0.001$	Casein kinase II	$F_{6,43}=15.8$ $P<0.001$
HNE3	$F_{6,43}=11.8$ $P<0.001$	Chitin synthase II	$F_{6,43}=82.4$ $P<0.001$
		Chitin synthase III	$F_{6,43}=12.7$ $P<0.001$

F ratios are given with the degrees of freedom for the factor effect and the error shown as a subscript. Significant effects ($P<0.05$) are in bold. The factor effect has seven levels (H1, H2, H3, H4 fractions, OME, central mantle and gills).

hemocytes (10^6 cells) were incubated for 30 min in 500 μ l of ASW with or without fluorescent beads (Nile Red FluoSpheres, 1.0 μ m, Invitrogen) at a 100:1 particles:hemocyte ratio. After incubation, cells were centrifuged at 250 *g* for 10 min to remove non-phagocytosed beads. Fluorescence signals were quantified using a BD LSRFortessa flow cytometer (BD Biosciences, San Jose, CA, USA) equipped with a 488 nm blue argon laser (i.e. 488 nm excitation wavelength) and the following bandpass filter/long pass (LP) dichroic mirror combinations: calcein AM 530/30, 505 LP; Nile Red FluoSphere 610/20, 600 LP. Linear, logarithmic fluorescence and scatter signal were recorded using 10^4 cells per analysis. Relative cell size and complexity were assessed by the forward scatter (FSC) and side scatter (SSC), respectively. Data were analysed using FlowJo version X software (FlowJo LLC, Ashland, OR, USA). All fluorescence data are expressed as relative fluorescence units (RU) per 10^4 cells.

Adhesion capacity

Isolated hemocytes (10^6 cells) were placed in 1 ml of ASW in the wells of a 12-well plate (Costar, Corning) and incubated for 2 h at room temperature. After the incubation, ASW was collected and the wells were surface-washed with 1 ml of ASW. The washes were combined with the previously collected ASW and centrifuged for 10 min at 1000 *g* to collect non-adhered cells. The non-adhered cells were counted using a Bright-Line hemacytometer (Sigma-Aldrich), and the adhesion capacity expressed as the percentage of adhered cells in the total hemocyte population in each well.

Cellular motility assays

Motility of different hemocyte fractions was assessed with a quantitative cell migration assay using ThinCert cell culture inserts (pore size 3.0 μ m) in CELLSTAR 24-well plates (Greiner Bio-One, Monroe, NC, USA). Potential chemotaxis of the hemocytes towards tissue extracts of the mantle (as a biomineralization site) and the

Table 3. ANOVA: effects of hemocyte fraction on the hemocyte function and Ca²⁺ concentrations in *Crassostrea gigas*

Function	Factor effect
Adhesion	$F_{3,15}=11.2$ $P=0.0004$
Cell migration	$F_{3,15}=3.1$ $P=0.06$
Free Ca ²⁺	$F_{3,15}=4.6$ $P=0.028$
Internal complexity	$F_{3,15}=1.8$ $P=0.218$
Cell size	$F_{3,15}=0.1$ $P=0.955$
Phagocytosis	$F_{3,15}=0.6$ $P=0.631$

F ratios are given with the degrees of freedom for the factor effect and the error shown as a subscript. Significant effects ($P<0.05$) are highlighted in bold. The factor effect has four levels (H1, H2, H3 and H4 fractions of hemocytes).

muscle (which contains a large hemolymph lacuna) were tested against the ASW control. Filter sterilized tissue extracts (10% mantle or 10% muscle extracts in ASW) were used as potential chemoattractants. In brief, 600 μ l of ASW with 2% glucose with or without a potential chemoattractant was placed in each well of the 24-well cell culture plate. Hemocyte suspension (200 μ l containing 2×10^5 cells) was placed onto the ThinCert membrane inserted into each well. The cells were incubated for 1 h, after which the ASW media was removed and replaced by 450 μ l of ASW with 8 μ mol l⁻¹ calcein-AM (Invitrogen). Cells were incubated for 45 min, after which the ThinCert inserts were transferred into freshly prepared cell culture wells containing 500 μ l of 0.125% trypsin-EDTA in ASW with 2% glucose and incubated for 10 min. This step led to the detachment of the cells that migrated to the outer surface of the ThinCert inserts. Because the pore size is smaller than the size of hemocytes, migration of the cells through the ThinCert membrane requires active motility mechanisms. Fluorescence of the detached cells was measured in trypsin-EDTA solution in a fluorescence plate reader (CytoFluor Series 4000, Framingham, MA, USA) (excitation: emission 485:520 nm) and expressed as the percentage of the total cell fluorescence (i.e. counting the cells migrated through the membrane and those retained inside the insert).

Statistical analyses

One-way ANOVA was used to test the effects of tissue type and/or hemocyte fraction on the studied traits (Tables 2, 3). Prior to analyses, data were tested for normality and homogeneity of variance by Kolmogorov–Smirnov and Levene's tests, respectively, and normalized as needed using Box–Cox common transforming method. Fisher's least significant differences (LSD) tests were used for planned *post hoc* comparisons of the differences between the pairs of means of interest. Principal component analysis (PCA) was used to determine the groups of traits that distinguish the different tissue types and/or hemocyte fractions using raw data. Normalized Box–Cox transformed data were subjected to the discriminant analysis to reduce the dimensionality of the multivariate data set and determine the grouping of the cell/tissue types in the multivariate trait space. All statistical analyses were performed with Statistica version 10.0 (StatSoft, USA). Differences were considered significant if the probability of type I error was less than 0.05. The data are presented as means \pm s.e.m. unless indicated otherwise.

RESULTS

Hemocyte morphology and functional characteristics

Differential centrifugation on discontinuous density gradient yielded four fractions of hemocytes based on their buoyant density (Fig. 1). The uppermost fraction (H1) generally consisted

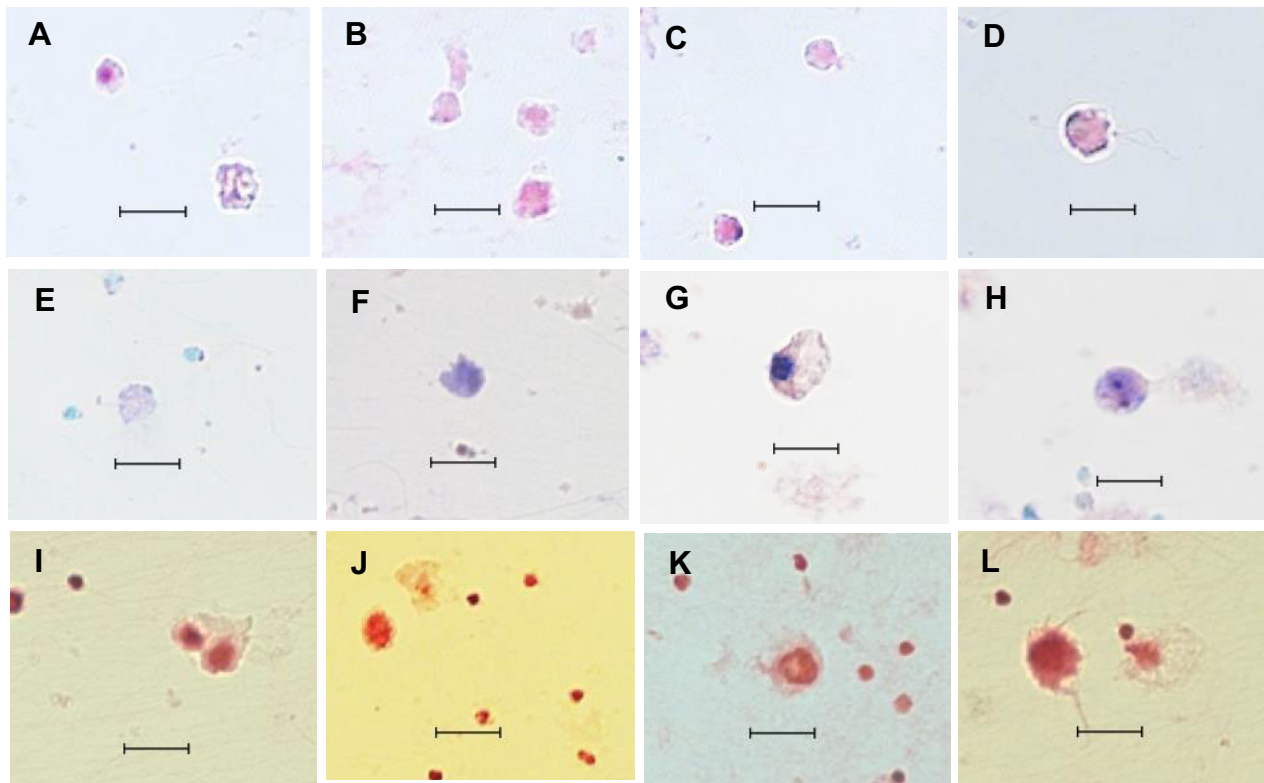


Fig. 1. Morphology of different hemocyte fractions. (A–D) Hematoxylin-eosin staining; (E–H) Wright–Giemsa staining; (I–L) Neutral Red staining. (A,E,I) Fraction H1; (B,F,J) fraction H2; (C,G,K) fraction H3; (D,H,L) fraction H4. Scale bars, 10 μ m.

of smaller spheroid cells with long filamentous pseudopodia (Fig. 1). The least buoyant H4 fraction contained cells of similar morphology to H1 but slightly larger in size (Fig. 1). Cell fractions H2 and H3 consisted of irregularly shaped cells with no filamentous structures on the surface (Fig. 1). Hemocyte fractions H1 and H4 had the highest adhesion capacity and motility (when measured in ASW) of the four studied fractions (Fig. 2A,B, Table 3). Presence of the muscle or mantle extract in the ASW (as a potential chemoattractant) slightly but notably inhibited hemocyte

movement, and the differences in motility among hemocytes from the four studied fractions disappeared (data not shown). Hemocytes from all four fractions were capable of phagocytosis, and no differences in the phagocytosis rates were found among the fractions (Fig. S1). Based on the side scatter in the flow cytometry, H4 fraction had the highest degree of granularity and/or internal complexity compared with other hemocytes fractions (Fig. 2C). Free calcium measured by flow cytometry was significantly higher in H2 hemocytes compared with other hemocyte fractions (Fig. 2D).

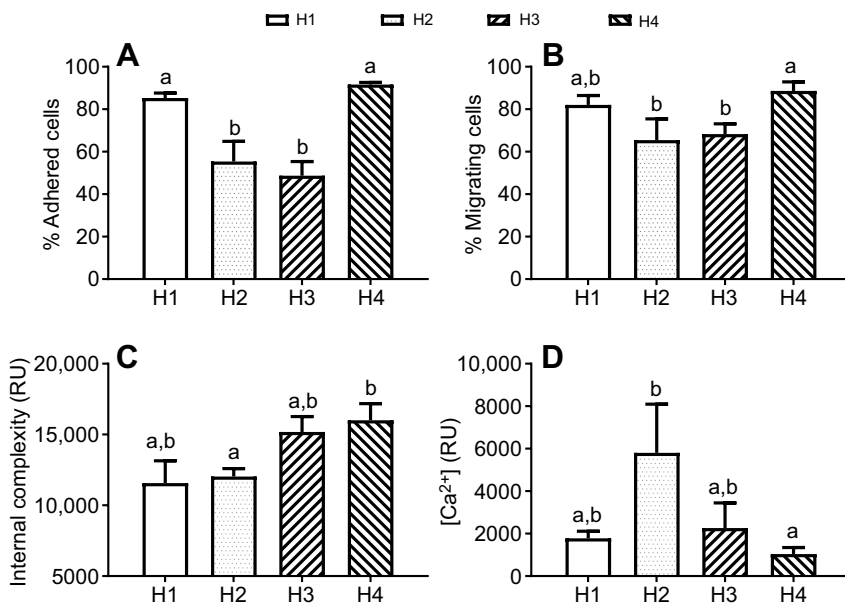


Fig. 2. Morphological and functional traits of different subpopulations of *Crassostrea gigas* hemocytes. (A) Cell adhesion capacity; (B) cell motility; (C) internal complexity measured by the side scatter on the flow cytometer; (D) [Ca²⁺]_i, measured calcein-AM fluorescence. RU, relative units. Different letters indicate values that are significantly different from each other ($P < 0.05$); $N = 4–5$.

Ion and acid–base homeostasis

mRNA expression profiles of genes involved in ion and acid–base regulation profoundly differed in hemocytes and mantle tissues of *C. gigas* (Table 2). Of the five studied carbonic anhydrase (CA) isoforms, CA XIV was almost exclusively expressed in the mantle (~35–39 CA XIV to β -actin ratios), with considerably lower expression levels in the gills (~1.3 CA XIV to β -actin ratios) or the hemocytes (~0.06–0.27 CA XIV to β -actin ratios) (Fig. 3E; Fig. S2). CA I, CA II, CA II and CA VII isoforms were more highly expressed in the hemocytes than in the gills or mantle, with distinctive expression patterns in different hemocyte fractions. Thus H1 and H4 fractions predominantly expressed CA I isoform, whilst H2 and H3 fractions had the highest expression of CA II, followed (in decreasing order) by CA I, CA III and CA VII isoforms (Fig. 3A–D; Fig. S2). Expression levels of V-type H^+ -ATPase and Ca^{2+} -ATPase type 2C were highest in the mantle edge and significantly lower in the central part of the mantle and in most of the hemocyte fractions (except Ca^{2+} -ATPase type 2C in H3, which was similar to the expression levels in the mantle edge) (Fig. 1F). In contrast, mRNA expression of the plasma membrane Ca^{2+} -ATPase (PMCA), NHX9 and NHE3 was significantly higher in the hemocytes than in the mantle (Fig. 3H–J). No significant differences in the expression of V-type H^+ ATPase, PMCA, NHX9 or NHE3 were found between different fractions of the hemocytes (Fig. 3). Notably, mRNA expression levels of V-type H^+ -ATPase, Ca^{2+} -ATPase (both type 2C and plasma membrane isoforms) as well as NHX9 and NHE3 in the gills were comparable with those in the biomineralizing tissues such as the mantle (Fig. 3).

ECM-related genes

Matrix protein-related genes (SLP, fibronectin, nacrein, casein kinase and chitin synthase isoforms), as well as VEGF and VEGF-R, were more highly expressed in the OME compared with the central part of the mantle (Figs 4 and 5). Of these, SLP and fibronectin Prot2L were especially strongly represented in the mantle edge (~30,000 and 128 target to β -actin ratios, respectively) (Fig. 4A,B). The respective ratios in the central mantle were 255 and 4 for SLP and fibronectin Prot2L. SLP and fibronectin Prot2L were not strongly expressed in the hemocytes (1–7 and 0.1–1 target to β -actin ratios, respectively) or in the gills (8 and 0.5 target to β -actin ratios, respectively) (Fig. 4A,B).

Fibronectin Prot3L and fibronectin ankyrin had higher expression in H2 and H3 fractions of the hemocytes, compared with H1 and H4 fractions, mantle or the gills (Fig. 4C,D). mRNA levels of nacrein, casein kinase I and casein kinase II were the highest in the H3 fraction of the hemocytes compared with all other studied tissues (Figs 4E and 5C,D). Chitin synthase isoforms showed a tissue-specific expression pattern, with chitin synthase II predominantly expressed in the mantle (especially the OME), and chitin synthase III in the hemocytes (Fig. 5E,F). VEGF and VEGF-R expression was the highest in the mantle edge and the gills and considerably lower in the hemocytes and the central mantle (Fig. 5A,B).

Multivariate analyses of gene expression profiles

PCA clearly separated different hemocyte fractions and tissue types based on the gene expression profiles (Fig. 6). Two first principal components (PC1 and PC2) explained 32 and 22% of the total data variance, respectively. All hemocyte fractions had high positive loadings on PC1, whereas the mantle and the gills had negative loadings on PC1. Notably, H1 and H4 were grouped together in the plane of the two first principal components and were associated with high loadings of CA I, CA VII and chitin synthase III (Fig. 6A).

Hemocyte fractions H2 and H3 were also grouped together, with high loadings of CA II and CA III, ion regulatory genes (NHX9, NHE3 and PM Ca^{2+} -ATPase), fibronectin Prot3L, fibronectin ankyrin and casein kinase I and II (Fig. 6A). Mantle edge was positioned in the opposite quadrant of the PC plane compared with the hemocytes and was associated with the expression of SLP, fibronectin Prot2L, chitin synthase II, VEGF, VEGF-R and Ca^{2+} -ATPase type 2C (Fig. 6A). The central part of the mantle and the gill were grouped together and separately from the mantle edge and hemocytes (Fig. 6A).

The discriminant analysis confirmed the results of the PCA and showed close grouping of H1 with H4, as well as H2 and H3 based on the gene expression patterns (Fig. 6B). All other tissue types (mantle edge, mantle center and the gills) were located separately from each other and from the hemocytes in the plane of the two first discriminant roots (Fig. 6B). The traits most closely associated with the discriminant function separating the groups included CA XIV, fibronectin Prot2L, VEGF, SLP and chitin synthase II ($P < 0.05$ for all traits; $F_{26,140} = 19.26$; $P < 0.0001$ for the discriminant function).

DISCUSSION

The high expression of a number of biomineralization-related genes in oyster hemocytes and mantle tissue indicates the important role of these cell types in biomineralization. Notably, different subpopulations of oyster hemocytes as well as different regions of the mantle reveal considerable functional specialization shown by the marked differences in gene expression profiles (Fig. 6). In general, expression of soluble CAs was higher in hemocytes, while membrane-associated CA XIV was expressed almost exclusively in the mantle. Furthermore, ion transporters (PM Ca^{2+} -ATPase, NHE3 and NHE9) were overexpressed in hemocytes, while ECM-associated proteins (SLP and fibronectin Prot2L) had higher expression levels in the mantle. These findings support the notion that hemocytes and mantle tissues play distinct roles in shell formation.

Functional diversity of oyster hemocytes

Morphological diversity of hemocytes that includes cells of different sizes and internal complexity (commonly defined as granulocytes, agranulocytes, and/or hyalinocytes) is a well-known trait of bivalves, including oysters (Foley and Cheng, 1977; Kennedy et al., 1996; Allam et al., 2002; Hegaret et al., 2003). However, the functional differentiation of hemocytes remains elusive, owing in part to difficulties of separating different subpopulations of live hemocytes for functional analysis (Goedken and De Guise, 2004; Terahara et al., 2006; Wang et al., 2017a). Our approach based on the separation of oyster hemocytes by their floating density revealed two functionally and morphologically distinct groups of cells, one including H1 and H4 fractions, and another one including H2 and H3 fractions (Fig. 6A). Hemocytes from H1 and H4 fractions consist of highly motile cells with well-developed pseudopodia and high adhesion capacity. Compared with the H2 and H3 fractions, these cells tend to have lower expression of V-type H^+ -ATPase, Ca^{2+} -ATPase, casein kinases I and II, chitin synthase II, nacrein and fibronectin Prot2L. Of the genes involved in ECM formation, only chitin synthase III is expressed at relatively high levels in H1 and H4 hemocytes. The expression profile of soluble CAs also differs between the H1 and H4 fractions (that express high levels of CA I and CA VII) and H2 and H3 fractions (expressing mainly CA II and CA III). The functional consequences of these differences in gene expression profiles between different hemocyte fractions are not fully understood. However, based on high motility and capacity to adhere to foreign materials (such as plastic), as well as the low expression of

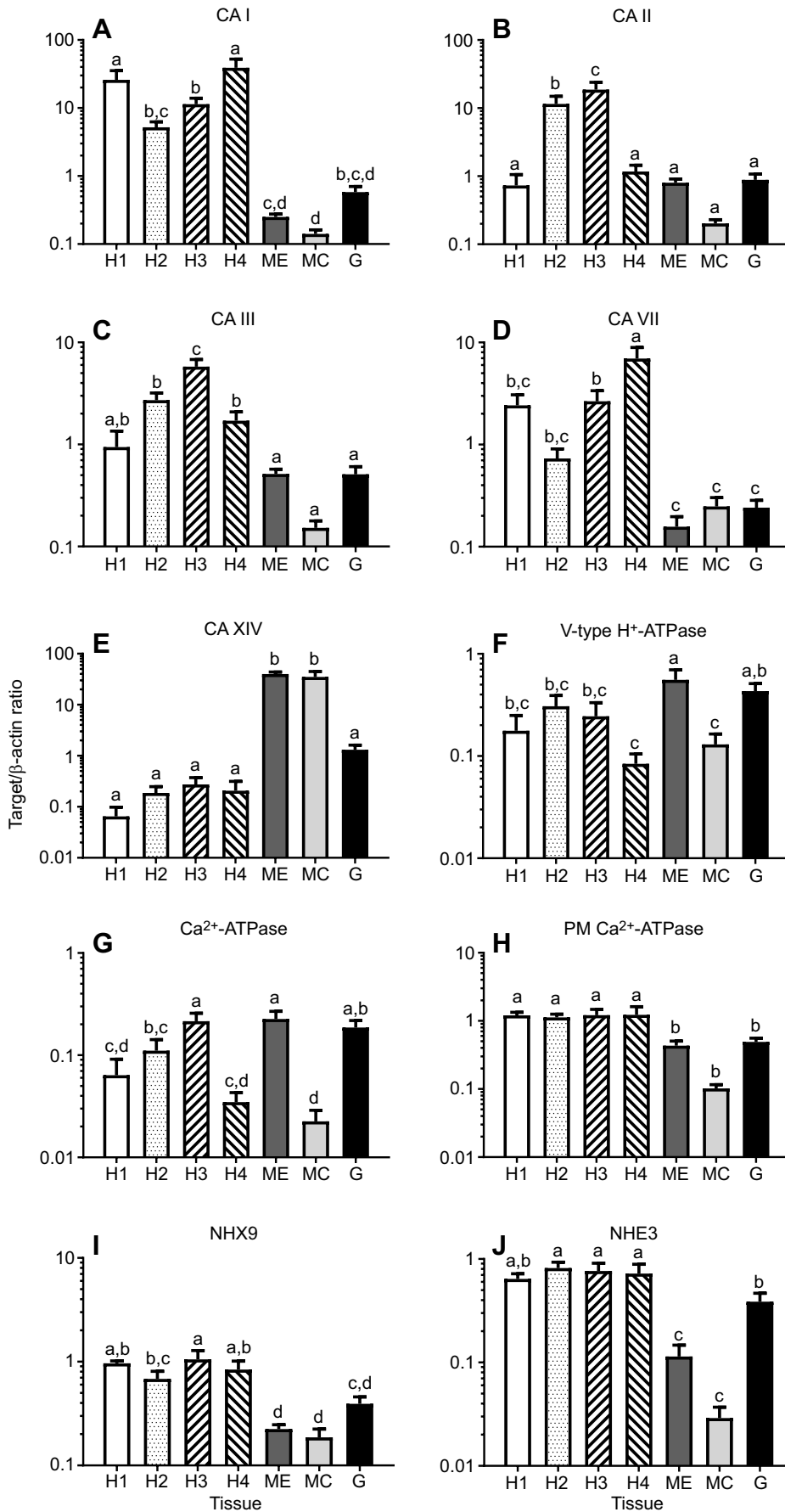


Fig. 3. Expression of mRNA of genes involved in ion and acid–base regulation in different hemocyte fractions and mantle and gill tissues of *C. gigas*. x-axis: tissue type and/or hemocyte fraction; y-axis: mRNA levels of the target gene relative to β-actin. H1–H4, different fractions of hemocytes; ME, outer mantle edge; MC, central part of the mantle; G, gills. Different letters indicate significant differences between the means for different tissues/fractions ($P < 0.05$). Vertical bars represent the standard error of means; $N = 6–9$ except H1 where $N = 4$.

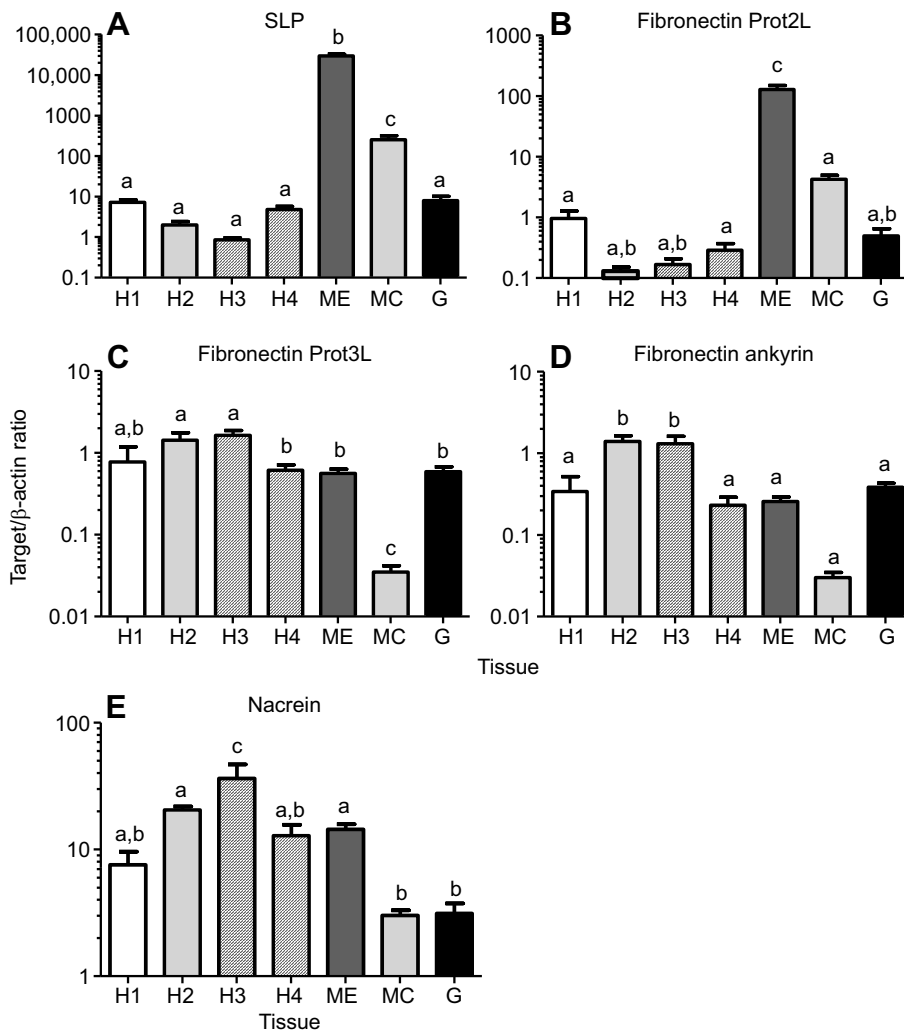


Fig. 4. Expression of mRNA of genes encoding scaffold proteins in different hemocyte fractions and mantle and gill tissues of *C. gigas*. x-axis: tissue type and/or hemocytes fraction; y-axis: mRNA levels of the target gene relative to β -actin. H1–H4, different fractions of hemocytes; ME, outer mantle edge; MC, central part of the mantle; G, gills. Different letters indicate significant differences between the means for different tissues/fractions ($P < 0.05$). Vertical bars represent the standard error of means. $N = 6$ –9 except H1 where $N = 4$.

biomineralization-related genes in H1 and H4 hemocytes, it appears that these cells are likely to be specialized on immune-related functions rather than on biomineralization. This conclusion is supported by a recent study in *C. gigas* showing that large hemocytes (corresponding to the H4 fraction in our present study) have considerably higher phagocytic and encapsulation capacity, as well as higher expression of immune-related genes (including the Toll-like receptor, clathrin, lysozyme and defensin) compared with other hemocyte fractions (Wang et al., 2017a). Taken together, these data indicate that H4 cells (~large granulocytes) represent the main immunocompetent cells in oysters. Hemocytes from the H1 fraction that share a strong similarity in gene expression profile and functional characteristics with the H4 fraction but are smaller and less internally complex, might represent progenitor cells of the H4 fraction. Further investigations of the hematopoiesis of oysters are required to test this hypothesis and determine whether the functional similarities between H1 and H4 fractions are the result of independent differentiation or reflect different stages of the same subpopulation of immunocompetent cells.

In contrast to H1 and H4 hemocytes, cells from the H2 and H3 fractions lack prominent pseudopodia and are less motile and adherent. Although H2 and H3 cells also predominantly express mRNA for soluble (cytosolic) isoforms of CA, the CA expression profile is different from H1 and H4 hemocytes. The most highly expressed isoform of CA in H2 and H3 hemocytes is CAII, which has

high catalytic activity in mammalian systems (Sly and Hu, 1995; Earnhardt et al., 1998). Notably, a recent report shows that the expression of CA II in oyster tissues (including hemocytes and to a lesser degree mantle) is significantly affected by changes in P_{CO_2} and indicates that this enzyme plays a prominent role in the regulation of carbonate chemistry, and thus biomineralization (Wang et al., 2017b). H2 hemocytes also have considerably higher $[Ca^{2+}]_i$ levels (revealed by calcein AM staining) compared with other hemocyte fractions, indicating their potential role in Ca^{2+} transport to biomineralization sites (Mount et al., 2004). Notably, H2 and H3 hemocytes express many genes potentially associated with biomineralization, including SLP, casein kinases, chitin synthases, VEGF, VEGF-R and nacrein-like protein. Interestingly, nacrein is usually associated with the aragonitic nacre layer of the shell in molluscs, such as the pearl oyster or turbinid gastropods (Marin and Luquet, 2004), and is believed to shift the crystallization reactions towards less thermodynamically stable aragonite (Kono et al., 2000; Norizuki and Samata, 2008). However, the function of nacrein-like proteins in Pacific oysters that build the adult shell exclusively from calcite is not clear. As nacrein-like protein contains a CA catalytic domain, it can potentially act as an extracellular CA (Song et al., 2014). However, the major difference between nacreins and nacrein-like proteins of Pacific oysters is that the latter contain a large number of acidic amino acids (Song et al., 2014), a hallmark of the matrix proteins associated with calcitic layers of bivalve shells (Tsukamoto

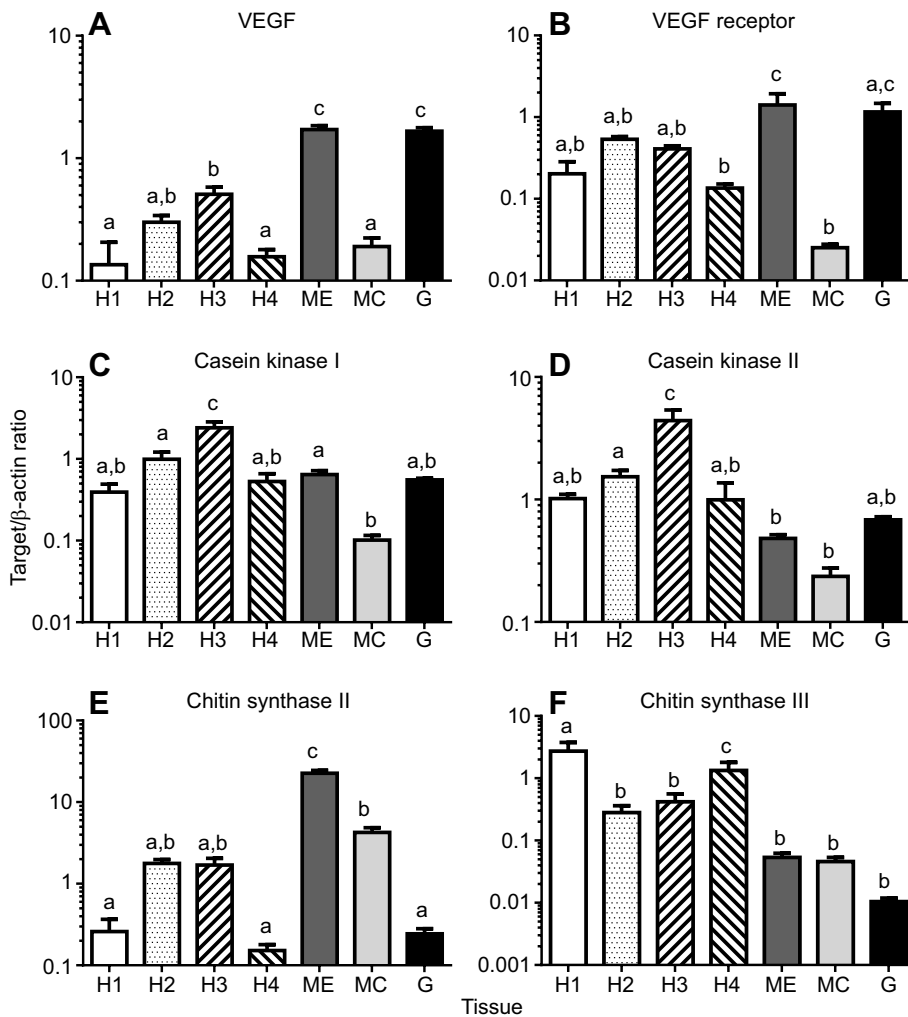


Fig. 5. Expression of mRNA of biomineralization-related genes, VEGF and VEGF receptor in different hemocyte fractions and mantle and gill tissues of *C. gigas*. x-axis: tissue type and/or hemocytes fraction; y-axis: mRNA levels of the target gene relative to β -actin. H1–H4, different fractions of hemocytes; ME, outer mantle edge; MC, central part of the mantle; G, gills; VEGF, vascular endothelial growth factor. Different letters indicate significant differences between the means for different tissues/fractions ($P < 0.05$). Vertical bars represent the standard error of means. $N = 6–9$ except H1 where $N = 4$.

et al., 2004; Gotliv et al., 2005; Marin et al., 2005). It is therefore possible that the nacrein-like proteins are involved in stabilization of amorphous calcium carbonate in hemocytes or modulation of calcite formation in the areas of active shell growth, as has been shown for other acidic mollusc proteins (Politi et al., 2007; Ndao et al., 2010).

Expression of casein kinase I and II mRNA was higher in H3 hemocytes than in other hemocyte fractions, the mantle or the gills. In vertebrates, casein kinases are involved in phosphorylation of secreted multi-phosphorylated proteins, involved in biomineralization (Sfeir and Veis, 1996; Veis et al., 1997; Sfeir et al., 2014). Earlier studies demonstrated the presence of highly phosphorylated proteins in shells (Rusenko et al., 1991) and hemocytes (Johnstone et al., 2008) of oysters, which may explain the high expression of casein kinases in oyster hemocytes. Notably, proteome of the hemocytes of a pearl oyster *Pinctada fucata* was also enriched for proteins involved in ECM formation and maturation including chitin synthase and tyrosinase; however, in this study the total hemocyte population was investigated without separation into functional or morphological subgroups (Li et al., 2016). The present study shows that hemocytes from H2 and H3 fractions express high levels of mRNA encoding fibronectins (fibronectin Prot3L and fibronectin-ankyrin), glycoproteins that play a key role in cell–cell interactions, cellular attachment as well as processes such as wound healing (Lenselink, 2015). Close interactions of hemocytes with the mantle-produced ECM and/or the mantle cells have been previously

documented in oysters undergoing shell repair (Li et al., 2016) or during the formation of the shell on artificial metallic implants (Johnstone et al., 2015). Our present observation of high expression of fibronectin-like proteins in hemocytes provides a potential molecular mechanism for these interactions. Taken together, these traits characterize H2 and H3 hemocytes as the likely players in biomineralization processes. Interestingly, high expression of nacrein-like protein and casein kinases in oyster hemocytes challenges the view that the shell proteins are exclusively produced by the mantle (Addadi et al., 2006; Jackson et al., 2006; Furuhashi et al., 2009; Clark et al., 2010) and indicates that in addition to mineral transport (Mount et al., 2004; Johnstone et al., 2015; Li et al., 2016), hemocytes may contribute to the formation of the shell organic matrix in oysters. This hypothesis is also supported by a recent transcriptomic study of *C. gigas* showing mRNA expression of several shell proteins in hemocytes (Wang et al., 2013).

Ionoregulatory pathways, including H^+ , Ca^{2+} and Na^+ transport, were highly represented in the transcriptome of all hemocyte fractions of *C. gigas*. mRNA expression levels of the plasma membrane Ca^{2+} -ATPase (involved in intracellular Ca^{2+} uptake) and Na^+/H^+ antiporters NHE3 and NHX9 (essential for intracellular pH regulation) in hemocytes exceeded those found in the mantle and gill tissues, while V-type H^+ -ATPase and Ca^{2+} -ATPase had similarly high expression levels in the hemocytes, OME and gills.

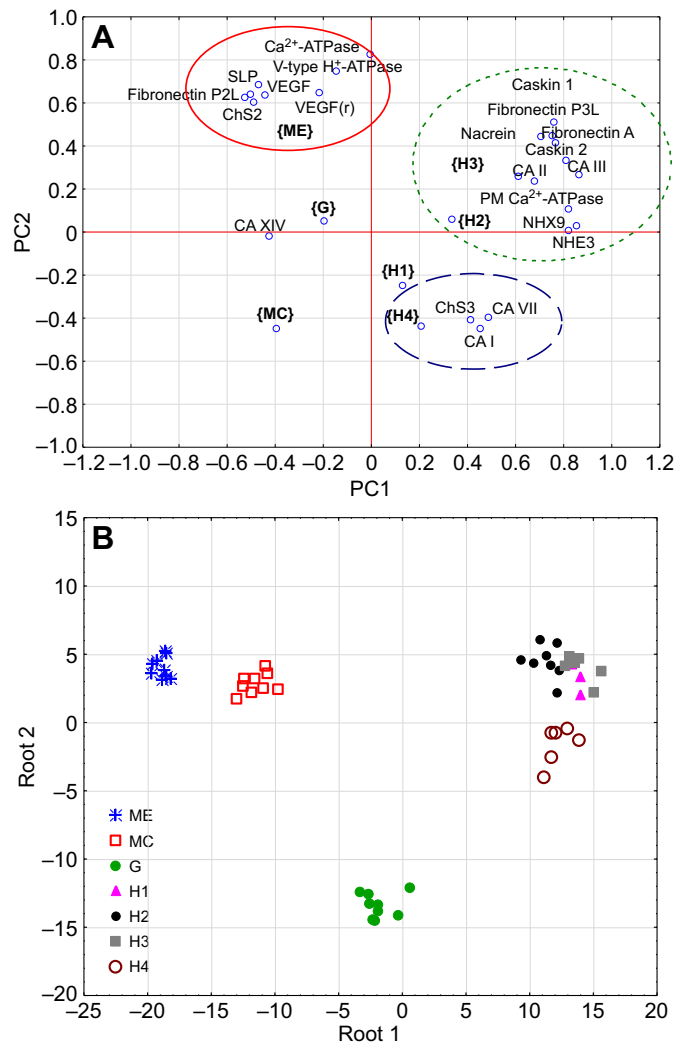


Fig. 6. Separation of the studied tissues/hemocyte fractions and genetic traits based on the PCA and discriminant analyses. (A) Position of the studied tissue types/hemocyte fractions and the genetic traits in the plane of the two first principal components (PC) based on the PCA. (B) Groupings of individual samples from different tissue types and hemocyte fractions based on discriminant analysis. H1–H4, different fractions of hemocytes; ME, outer mantle edge; MC, central part of the mantle; G, gills; CA, carbonic anhydrase; ChS, chitin synthase; SLP, silk-like protein; VEGF, vascular endothelial growth factor; Fibronectin A, fibronectin ankyrin. The traits most closely associated with the discriminant function included CA II, CA III, CA VII, VEGF, nacrein and chitin synthase III.

All hemocyte subpopulations isolated in this study were capable of phagocytosis. This observation agrees with the earlier findings that different types of oyster hemocytes (granulocytes, hyalinocytes and/or agranulocytes) have phagocytic ability (Takahashi and Mori, 2000; Terahara et al., 2006), albeit some studies indicate that granulocytes and hyalinocytes may exhibit different phagocytosis rates (Goedken and De Guise, 2004; Terahara et al., 2006) as well as different molecular mechanisms of phagocytosis (Terahara et al., 2006). Overall, our findings indicate similarity and/or functional redundancy between different hemocyte subpopulations with regard to some immune functions and ion regulation.

Local gene expression patterns in oyster mantle

The OME showed high expression of the biomineralization-related genes, often considerably higher than that in the central mantle or

hemocytes. Compared with other tissue types, mRNA encoding for the ECM-related proteins (SLP and chitin synthase II) and cell–cell interactions (VEGF, VEGF-R and fibronectin Prot2L) demonstrated higher levels of expression in the OME (Fig. 6). This observation is in agreement with the current paradigm stating that the mantle edge is primarily responsible for the ECM deposition and regulation of shell formation (Marin et al., 2008). Gene expression profiles of the OME indicate the strong involvement of this part of the mantle in production of ECM proteins. Thus, SLP had the highest expression in OME, with mRNA levels ~115-fold higher than in the central mantle, and ~4000- to 34,000-fold higher than in hemocytes. Hydrophobic silk-like proteins, along with chitin, are the major component of the shell protein matrix, which organizes and guides the formation of CaCO₃ crystals in the molluscan shell (Addadi et al., 2006; Joubert et al., 2010). Nacrein mRNA levels were ~5-fold higher in the OME than in H2 and H3 hemocytes. Chitin synthase II mRNA levels in OME were ~5-fold higher than in the central mantle, ~12-fold higher than in the putatively biomineralizing hemocytes (H2 and H3) and ~90- to 150-fold higher than in non-biomineralizing tissues (gills or H1 and H4 hemocytes). Elevated expression of ECM proteins (such as shematrins, structural glycoproteins of the shell matrix, and lysine-rich matrix proteins of the KRMP family) were also shown in the OME of a pearl oyster *Pinctada fucata* (Gardner et al., 2011). In the present study, OME of *C. gigas* also showed high mRNA levels of fibronectin Prot2L, suggesting that this part of the mantle may be responsible for interactions of the shell ECM with biomineralizing hemocytes. Importantly, overexpression of fibronectin Prot2L mRNA is associated with the onset of shell formation during the larval development of *C. gigas*, indicating an important role of this protein in biomineralization (Zhang et al., 2012).

The OME also expressed high mRNA levels of ionoregulatory genes, including V-type H⁺-ATPase, Ca²⁺ transporters (including Ca²⁺-transporting ATPase type 2C and plasma membrane Ca²⁺-ATPase) and Na⁺/H⁺ antiporters NHE3 and NHX9. mRNA expression levels of these proteins in the OME were similar to those found in the gill, the main ionoregulatory organ of bivalves (albeit lower than in the hemocytes). This suggests that in addition to its role in the synthesis and maturation of the ECM, the OME contributes to the regulation of the ion and acid–base balance of the pallium, including the biomineralization site. Unlike hemocytes that predominantly expressed soluble CA, the major type of CA expressed in the mantle was the transmembrane isoform CA XIV. Levels of CA XIV mRNA in the mantle were ~30-fold higher than in the gills, and ~150- to 600-fold higher than in hemocytes. This indicates involvement of the mantle tissue in the maintenance of the acid–base balance in the pallium, as the membrane-bound CAs play a key role in the regulation of the bicarbonate and proton concentrations in extracellular fluids (Henry, 1996).

Expression levels of VEGF and VEGF-R mRNA were considerably higher in the OME compared with the central mantle (by ~9-fold and ~56-fold for VEGF and VEGF-R, respectively) or hemocytes (by ~3- to 12-fold and ~3- to 10-fold for VEGF and VEGF-R, respectively). Notably, gill tissues also had high levels of mRNA expression of VEGF and VEGF-R, similar to those found in the OME. VEGF is a multifunctional protein best known for its role in the regulation of angiogenesis and osteogenesis (Dai and Rabie, 2007; Duan et al., 2016) in vertebrates; however, it is evolutionarily conserved in different groups of animals, including those that, like molluscs, lack a closed circulatory system (Kipryushina et al., 2015). Recent studies suggested that VEGF and its receptor play an

important role of biomineralization in marine invertebrates, such as sea urchins, where VEGF regulates and directs migration of primary mesenchymal cells (PMC) involved in skeletogenesis (Duloquin et al., 2007; Adomako-Ankomah and Etensohn, 2014) and regulates growth of the calcitic spicules (Knapp et al., 2012). VEGF regulates expression of biomineralization-related genes in PMC of sea urchins, whilst inhibition of VEGF suppresses spiculogenesis (Duloquin et al., 2007; Sun and Etensohn, 2014). The cell-guiding function of VEGF appears to be conserved in different animals, as shown by the important role of the VEGF homologs in the migration of *Drosophila* hemocytes (Parsons and Foley, 2013) and recruitment of macrophages into the growing mammalian bone (Hu and Olsen, 2016). Notably, when compared between different fractions of oyster hemocytes, the putative biomineralizing hemocytes (H2 and H3) tend to express higher VEGF and VEGF-R mRNA levels than their non-biomineralizing counterparts (H1 and H4). This, along with the elevated expression of VEGF and VEGF-R mRNA in the OME of *C. gigas*, points towards the potentially important role of cell-surface receptors and cell–cell interactions between the OME and hemocytes at the biomineralization site.

Conclusions and perspectives

Our study shows considerable functional specialization (revealed by the gene expression patterns and/or functional characteristics in the cells) between biomineralizing tissues (i.e. hemocytes versus mantle) and within each tissue type (i.e. between different hemocyte fractions or different regions of the mantle). Spatial organization and functional specialization of the different parts of oyster mantle supports the earlier proposed important role of the OME in shell formation including production of the shell protein matrix and interaction with other cells (i.e. hemocytes) involved in biomineralization. Notably, our data indicate that hemocytes may contribute to the formation of the ECM in addition to their proposed role in mineral transport (Mount et al., 2004; Li et al., 2016), and challenge the current paradigm of the mantle as the sole source of the ECM for shell formation. Variation in the expression patterns of biomineralization-related genes combined with differences in the motility and adhesion between different hemocyte fractions demonstrate that different types of hemocytes are predominantly engaged in shell production and/or the immune response. Further studies are needed to determine to what degree the functional specialization of hemocytes reflects cell differentiation, or whether it is flexible depending on the hemocyte age and/or the functional state of the oyster. The mechanisms of cell–cell interactions between hemocytes and the OME (such as those involving fibronectins of VEGF) at the biomineralization front represent another exciting and potentially fruitful field of study. Overall, our findings demonstrate the multifunctional roles of hemocytes and mantle tissues in biomineralization and emphasize complexity of the biological controls over shell formation in bivalves.

Acknowledgements

The authors thank Dr David Foureau (Carolina HealthCare System) for the help with the flow cytometry.

Competing interests

The authors declare no competing or financial interests.

Author contributions

Conceptualization: A.V.I., E.B., I.M.S.; Methodology: A.V.I., H.I.F., E.B., I.M.S.; Formal analysis: A.V.I., H.I.F., H.P., I.M.S.; Investigation: A.V.I., H.I.F.; Data curation: A.V.I., H.I.F., H.P.; Writing - original draft: A.V.I., E.B., I.M.S.; Writing - review & editing: A.V.I., H.I.F., H.P., E.B., I.M.S.; Visualization: H.I.F., I.M.S.; Supervision: I.M.S.; Project administration: I.M.S.; Funding acquisition: E.B., I.M.S.

Funding

This work was supported by the US National Science Foundation (awards IOS-1557870 and IOS-1557551 to I.M.S. and E.B.).

Supplementary information

Supplementary information available online at <http://jeb.biologists.org/lookup/doi/10.1242/jeb.160861.supplemental>

References

- Addadi, L., Joester, D., Nudelman, F. and Weiner, S. (2006). Mollusk shell formation: a source of new concepts for understanding biomineralization processes. *Chem. Eur. J.* **12**, 980–987.
- Adomako-Ankomah, A. and Etensohn, C. A. (2014). Growth factors and early mesoderm morphogenesis: insights from the sea urchin embryo. *Genesis* **52**, 158–172.
- Akiva, A., Malkinson, G., Masic, A., Kerschnitzki, M., Bennet, M., Fratzi, P., Addadi, L., Weiner, S. and Yaniv, K. (2015). On the pathway of mineral deposition in larval zebrafish caudal fin bone. *Bone* **75**, 192–200.
- Albeck, S., Aizenberg, J., Addadi, L. and Weiner, S. (1993). Interactions of various skeletal intracrystalline components with calcite crystals. *J. Am. Chem. Soc.* **115**, 11691–11697.
- Allam, B., Ashton-Alcox, K. A. and Ford, S. E. (2002). Flow cytometric comparison of haemocytes from three species of bivalve molluscs. *Fish Shellfish Immunol.* **13**, 141–158.
- Beniash, E., Addadi, L. and Weiner, S. (1999). Cellular control over spicule formation in sea urchin embryos: a structural approach. *J. Struct. Biol.* **125**, 50–62.
- Beniash, E., Ivanina, A., Lieb, N. S., Kurochkin, I. and Sokolova, I. M. (2010). Elevated level of carbon dioxide affects metabolism and shell formation in oysters *Crassostrea virginica* (Gmelin). *Mar. Ecol. Prog. Ser.* **419**, 95–108.
- Boonrungsiman, S., Gentleman, E., Carzaniga, R., Evans, N. D., McComb, D. W., Porter, A. E. and Stevens, M. M. (2012). The role of intracellular calcium phosphate in osteoblast-mediated bone apatite formation. *Proc. Natl. Acad. Sci. USA* **109**, 14170–14175.
- Checa, A. G., Esteban-Delgado, F. J. and Rodríguez-Navarro, A. B. (2007). Crystallographic structure of the foliated calcite of bivalves. *J. Struct. Biol.* **157**, 393–402.
- Choi, C.-S. and Kim, Y.-W. (2000). A study of the correlation between organic matrices and nanocomposite materials in oyster shell formation. *Biomaterials* **21**, 213–222.
- Clark, M. S., Thorne, M. A. S., Vieira, F. A., Cardoso, J. C. R., Power, D. M. and Peck, L. S. (2010). Insights into shell deposition in the Antarctic bivalve *Laternula elliptica*: gene discovery in the mantle transcriptome using 454 pyrosequencing. *BMC Genomics* **11**, 362.
- Crenshaw, M. A. (1972). The inorganic composition of molluscan extrapallial fluid. *Biol. Bull.* **143**, 506–512.
- Dai, J. and Rabie, A. B. M. (2007). VEGF: an essential mediator of both angiogenesis and endochondral ossification. *J. Dent. Res.* **86**, 937–950.
- Dauphin, Y., Ball, A. D., Castillo-Michel, H., Chevillard, C., Cuif, J.-P., Farre, B., Pouvreau, S. and Salomé, M. (2013). *In situ* distribution and characterization of the organic content of the oyster shell *Crassostrea gigas* (Mollusca, Bivalvia). *Micron* **44**, 373–383.
- Dickinson, G. H., Ivanina, A. V., Matoo, O. B., Pörtner, H. O., Lannig, G., Bock, C., Beniash, E. and Sokolova, I. M. (2012). Interactive effects of salinity and elevated CO₂ levels on juvenile eastern oysters, *Crassostrea virginica*. *J. Exp. Biol.* **215**, 29–43.
- Dickinson, G. H., Matoo, O. B., Tourek, R. T., Sokolova, I. M. and Beniash, E. (2013). Environmental salinity modulates the effects of elevated CO₂ levels on juvenile hard-shell clams, *Mercenaria mercenaria*. *J. Exp. Biol.* **216**, 2607–2618.
- Duan, X., Bradbury, S. R., Olsen, B. R. and Berendsen, A. D. (2016). VEGF stimulates intramembranous bone formation during craniofacial skeletal development. *Matrix Biol.* **52–54**, 127–140.
- Duloquin, L., Lhomond, G. and Gache, C. (2007). Localized VEGF signaling from ectoderm to mesenchyme cells controls morphogenesis of the sea urchin embryo skeleton. *Development* **134**, 2293–2302.
- Earnhardt, J. N., Qian, M., Tu, C., Lakkis, M. M., Bergenhem, N. C. H., Laipis, P. J., Tashian, R. E. and Silverman, D. N. (1998). The catalytic properties of murine carbonic anhydrase VII. *Biochemistry* **37**, 10837–10845.
- Falini, G., Albeck, S., Weiner, S. and Addadi, L. (1996). Control of aragonite or calcite polymorphism by mollusk shell macromolecules. *Science* **271**, 67–69.
- Fisher, W. S. (2004). Relationship of amebocytes and terrestrial elements to adult shell deposition in eastern oysters. *J. Shellfish Res.* **23**, 353–367.
- Foley, D. A. and Cheng, T. C. (1977). Degranulation and other changes of molluscan granulocytes associated with phagocytosis. *J. Invertebr. Pathol.* **29**, 321–325.
- Furuhashi, T., Schwarzing, C., Miksik, I., Smrz, M. and Beran, A. (2009). Molluscan shell evolution with review of shell calcification hypothesis. *Comp. Biochem. Physiol. B Biochem. Mol. Biol.* **154**, 351–371.

- Gardner, L. D., Mills, D., Wiegand, A., Leavesley, D. and Elizur, A. (2011). Spatial analysis of biomineralization associated gene expression from the mantle organ of the pearl oyster *Pinctada maxima*. *BMC Genomics* **12**, 455.
- Goedken, M. and De Guise, S. (2004). Flow cytometry as a tool to quantify oyster defence mechanisms. *Fish Shellfish Immunol.* **16**, 539–552.
- Gotliv, B.-A., Kessler, N., Sumerel, J. L., Morse, D. E., Tuross, N., Addadi, L. and Weiner, S. (2005). Asprich: a novel aspartic acid-rich protein family from the prismatic shell matrix of the bivalve *Atrina rigida*. *Chembiochem* **6**, 304–314.
- Gutiérrez, J. L., Jones, C. G., Strayer, D. L. and Iribarne, O. O. (2003). Mollusks as ecosystem engineers: the role of shell production in aquatic habitats. *Oikos* **101**, 79–90.
- Haszprunar, G. and Wanninger, A. (2012). Molluscs. *Curr. Biol.* **22**, R510–R514.
- Hegaret, H., Wikfors, G. H. and Soudant, P. (2003). Flow cytometric analysis of haemocytes from eastern oysters, *Crassostrea virginica*, subjected to a sudden temperature elevation: II. Haemocyte functions: aggregation, viability, phagocytosis, and respiratory burst. *J. Exp. Mar. Biol. Ecol.* **293**, 249–265.
- Henry, R. P. (1996). Multiple roles of carbonic anhydrase in cellular transport and metabolism. *Annu. Rev. Physiol.* **58**, 523.
- Hu, K. and Olsen, B. R. (2016). Osteoblast-derived VEGF regulates osteoblast differentiation and bone formation during bone repair. *J. Clin. Invest.* **126**, 509–526.
- Jackson, D., McDougall, C., Green, K., Simpson, F., Worheide, G. and Degnan, B. (2006). A rapidly evolving secretome builds and patterns a sea shell. *BMC Biol.* **4**.
- Jackson, D. J., McDougall, C., Woodcroft, B., Moase, P., Rose, R. A., Kube, M., Reinhardt, R., Rokhsar, D. S., Montagnani, C., Joubert, C. et al. (2010). Parallel evolution of nacre building gene sets in molluscs. *Mol. Biol. Evol.* **27**, 591–608.
- Jodrey, L. H. (1953). Studies on shell formation. III. Measurement of calcium deposition in shell and calcium turnover in mantle tissue using the mantle-shell preparation and Ca45. *Biol. Bull.* **104**, 398–407.
- Johnstone, M. B., Ellis, S., Mount, A. S. (2008). Visualization of shell matrix proteins in hemocytes and tissues of the Eastern oyster, *Crassostrea virginica*. *J. Exp. Zool. B Mol. Dev. Evol.* **310B**, 227–239.
- Johnstone, M. B., Gohad, N. V., Falwell, E. P., Hansen, D. C., Hansen, K. M. and Mount, A. S. (2015). Cellular orchestrated biomineralization of crystalline composites on implant surfaces by the eastern oyster, *Crassostrea virginica* (Gmelin, 1791). *J. Exp. Mar. Biol. Ecol.* **463**, 8–16.
- Joubert, C., Piquemal, D., Marie, B., Manchon, L., Pierrat, F., Zanella-Cléon, I., Cochennec-Laureau, N., Gueguen, Y. and Montagnani, C. (2010). Transcriptome and proteome analysis of *Pinctada margaritifera* calcifying mantle and shell: focus on biomineralization. *BMC Genomics* **11**, 613.
- Kamat, S., Su, X., Ballarini, R. and Heuer, A. H. (2000). Structural basis for the fracture toughness of the shell of the conch *Strombus gigas*. *Nature* **405**, 1036–1040.
- Kennedy, V. S., Newell, R. I. E. and Eble, A. F. (ed.). (1996). *The Eastern Oyster Crassostrea virginica*. College Park, Maryland: A Maryland Sea Grant Book.
- Kipryushina, Y. O., Yakovlev, K. V. and Odintsova, N. A. (2015). Vascular endothelial growth factors: a comparison between invertebrates and vertebrates. *Cytokine Growth Factor. Rev.* **26**, 687–695.
- Knapp, R. T., Wu, C.-H., Mobilia, K. C. and Joester, D. (2012). Recombinant sea urchin vascular endothelial growth factor directs single-crystal growth and branching *in vitro*. *J. Am. Chem. Soc.* **134**, 17908–17911.
- Kocot, K. M., Aguilera, F., McDougall, C., Jackson, D. J. and Degnan, B. M. (2016). Sea shell diversity and rapidly evolving secretomes: insights into the evolution of biomineralization. *Front. Zool.* **13**, 23.
- Kono, M., Hayashi, N. and Samata, T. (2000). Molecular mechanism of the nacreous layer formation in *Pinctada maxima*. *Biochem. Biophys. Res. Commun.* **269**, 213–218.
- Lee, S. W., Kim, G. H. and Choi, C. S. (2008). Characteristic crystal orientation of folia in oyster shell, *Crassostrea gigas*. *Mater. Sci. Eng. C Biomim. Supramol. Syst.* **28**, 258–263.
- Lenselink, E. A. (2015). Role of fibronectin in normal wound healing. *Int. Wound J.* **12**, 313–316.
- Li, S., Liu, C., Huang, J., Liu, Y., Zhang, S., Zheng, G., Xie, L. and Zhang, R. (2016). Transcriptome and biomineralization responses of the pearl oyster *Pinctada fucata* to elevated CO₂ and temperature. *Sci. Rep.* **6**, 18943.
- Lowe, D. M. and Pipe, R. K. (1994). Contaminant induced lysosomal membrane damage in marine mussel digestive cells: an *in vitro* study. *Aquat. Toxicol.* **30**, 357–365.
- Mahamid, J., Sharif, A., Gur, D., Zelzer, E., Addadi, L. and Weiner, S. (2011). Bone mineralization proceeds through intracellular calcium phosphate loaded vesicles: a cryo-electron microscopy study. *J. Struct. Biol.* **174**, 527–535.
- Marie, B., Joubert, C., Tayale, A., Zanella-Cleon, I., Belliard, C., Piquemal, D., Cochennec-Laureau, N., Marin, F., Gueguen, Y. and Montagnani, C. (2012). Different secretory repertoires control the biomineralization processes of prism and nacre deposition of the pearl oyster shell. *Proc. Natl. Acad. Sci. USA* **109**, 20986–20991.
- Marin, F. and Luquet, G. (2004). Molluscan shell proteins. *Comptes Rendus Palevol* **3**, 469–492.
- Marin, F., Amons, R., Guichard, N., Stigter, M., Hecker, A., Luquet, G., Layrolle, P., Alcaraz, G., Riondet, C. and Westbroek, P. (2005). Caspartin and calprism, two proteins of the shell calcitic prisms of the Mediterranean fan mussel *Pinna nobilis*. *J. Biol. Chem.* **280**, 33895–33908.
- Marin, F., Luquet, G., Marie, B. and Medakovic, D. (2008). Molluscan shell proteins: primary structure, origin, and evolution. In *Current Topics in Developmental Biology*, Vol. 80 (ed. G. P. Schatten), pp. 209–276. New York: Academic Press.
- Mayer, G. and Sarikaya, M. (2002). Rigid biological composite materials: structural examples for biomimetic design. *Exp. Mech.* **42**, 395–403.
- Mount, A. S., Wheeler, A. P., Paradar, R. P. and Snider, D. (2004). Hemocyte-mediated shell mineralization in the eastern oyster. *Science* **304**, 297–300.
- Ndao, M., Keene, E., Amos, F. F., Rewari, G., Ponce, C. B., Estroff, L. and Evans, J. S. (2010). Intrinsically disordered mollusk shell prismatic protein that modulates calcium carbonate crystal growth. *Biomacromolecules* **11**, 2539–2544.
- Norizuki, M. and Samata, T. (2008). Distribution and function of the nacrein-related proteins inferred from structural analysis. *Mar. Biotechnol.* **10**, 234–241.
- Nudelman, F., Gotliv, B. A., Addadi, L. and Weiner, S. (2006). Mollusk shell formation: mapping the distribution of organic matrix components underlying a single aragonitic tablet in nacre. *J. Struct. Biol.* **153**, 176–187.
- Parsons, B. and Foley, E. (2013). The *Drosophila* PDGF and VEGF-receptor related (Pvr) ligands Pvf2 and Pvf3 control hemocyte viability and invasive migration. *J. Biol. Chem.* **288**, 20173–20183.
- Pfaffl, M. W. (2001). A new mathematical model for relative quantification in real-time RT-PCR. *Nucleic Acids Res.* **29**, 2002–2007.
- Politi, Y., Mahamid, J., Goldberg, H., Weiner, S. and Addadi, L. (2007). Asprich mollusk shell protein: *in vitro* experiments aimed at elucidating function in CaCO₃ crystallization. *Crystengcomm* **9**, 1171–1177.
- Ries, J. B., Cohen, A. L. and McCorkle, D. C. (2009). Marine calcifiers exhibit mixed responses to CO₂-induced ocean acidification. *Geology* **37**, 1131–1134.
- Rusenko, K. W., Donachy, J. E. and Wheeler, A. P. (1991). Purification and characterization of a shell matrix phosphoprotein from the American oyster. *ACS Symp. Ser.* **444**, 107–124.
- Sfeir, C. and Veis, A. (1996). The membrane associated kinases which phosphorylate bone and dentin extracellular matrix phosphoproteins are isoforms of cytosolic CKII. *Connect. Tissue Res.* **35**, 215–222.
- Sfeir, C., Fang, P.-A., Jayaraman, T., Raman, A., Xiaoyuan, Z. and Beniash, E. (2014). Synthesis of bone-like nanocomposites using multiphosphorylated peptides. *Acta Biomater.* **10**, 2241–2249.
- Sly, W. S. and Hu, P. Y. (1995). Human carbonic anhydrases and carbonic anhydrase deficiencies. *Annu. Rev. Biochem.* **64**, 375–401.
- Smith, B. L., Schäffer, T. E., Viani, M., Thompson, J. B., Frederick, N. A., Kindt, J., Belcher, A., Stucky, G. D., Morse, D. E. and Hansma, P. K. (1999). Molecular mechanistic origin of the toughness of natural adhesives, fibres and composites. *Nature* **399**, 761–763.
- Sokolova, I. M., Bock, C. and Pörtner, H.-O. (2000). Resistance to freshwater exposure in White Sea *Littorina* spp. II: acid-base regulation. *J. Comp. Physiol. B Biochem. Syst. Environ. Physiol.* **170**, 105–115.
- Song, X., Wang, X., Li, L. and Zhang, G. (2014). Identification two novel nacrein-like proteins involved in the shell formation of the Pacific oyster *Crassostrea gigas*. *Mol. Biol. Rep.* **41**, 4273–4278.
- Sun, Z. and Etensohn, C. A. (2014). Signal-dependent regulation of the sea urchin skeletogenic gene regulatory network. *Gene Expr. Patterns* **16**, 93–103.
- Takahashi, K. G. and Mori, K. (2000). Functional profiles of hemocytes in the bio-defense process of the Pacific oyster, *Crassostrea gigas*. *Tohoku J. Agric. Res.* **51**, 15–27.
- Terahara, K., Takahashi, K. G., Nakamura, A., Osada, M., Yoda, M., Hiroi, T., Hirasawa, M. and Mori, K. (2006). Differences in integrin-dependent phagocytosis among three hemocyte subpopulations of the Pacific oyster "*Crassostrea gigas*". *Dev. Comp. Immunol.* **30**, 667–683.
- Tsakamoto, D., Sarashina, I. and Endo, K. (2004). Structure and expression of an unusually acidic matrix protein of pearl oyster shells. *Biochem. Biophys. Res. Commun.* **320**, 1175–1180.
- Veis, A., Sfeir, C. and Wu, C. B. (1997). Phosphorylation of the proteins of the extracellular matrix of mineralized tissues by casein kinase-like activity. *Crit. Rev. Oral Biol. Med.* **8**, 360–379.
- Vidavsky, N., Addadi, S., Mahamid, J., Shimoni, E., Ben-Ezra, D., Shpigel, M., Weiner, S. and Addadi, L. (2014). Initial stages of calcium uptake and mineral deposition in sea urchin embryos. *Proc. Natl. Acad. Sci. USA* **111**, 39–44.
- Vidavsky, N., Masic, A., Schertel, A., Weiner, S. and Addadi, L. (2015). Mineral-bearing vesicle transport in sea urchin embryos. *J. Struct. Biol.* **192**, 358–365.
- Wang, X., Li, L., Zhu, Y., Du, Y., Song, X., Chen, Y., Huang, R., Que, H., Fang, X. and Zhang, G. (2013). Oyster shell proteins originate from multiple organs and their probable transport pathway to the shell formation front. *PLoS ONE* **8**, e66522.
- Wang, W., Li, M., Wang, L., Chen, H., Liu, Z., Jia, Z., Qiu, L. and Song, L. (2017a). The granulocytes are the main immunocompetent hemocytes in *Crassostrea gigas*. *Dev. Comp. Immunol.* **67**, 221–228.

- Wang, X., Wang, M., Jia, Z., Qiu, L., Wang, L., Zhang, A. and Song, L.** (2017b). A carbonic anhydrase serves as an important acid-base regulator in pacific oyster *Crassostrea gigas* exposed to elevated CO₂: implication for physiological responses of mollusk to ocean acidification. *Mar. Biotechnol.* **19**, 22–35.
- Weiner, S., Traub, W. and Parker, S. B.** (1984). Macromolecules in Mollusc shells and their functions in biomineralization [and discussion]. *Philos. Trans. R. Soc. Lond. B Biol. Sci.* **304**, 425–434.
- Wilbur, K. M. and Jodrey, L. H.** (1955). Studies on shell formation. V. The inhibition of shell formation by carbonic anhydrase inhibitors. *Biol. Bull.* **108**, 359–365.
- Zhang, C. and Zhang, R.** (2006). Matrix proteins in the outer shells of molluscs. *Mar. Biotechnol.* **8**, 572–586.
- Zhang, G., Fang, X., Guo, X., Li, L., Luo, R., Xu, F., Yang, P., Zhang, L., Wang, X., Qi, H. et al.** (2012). The oyster genome reveals stress adaptation and complexity of shell formation. *Nature* **490**, 49–54.

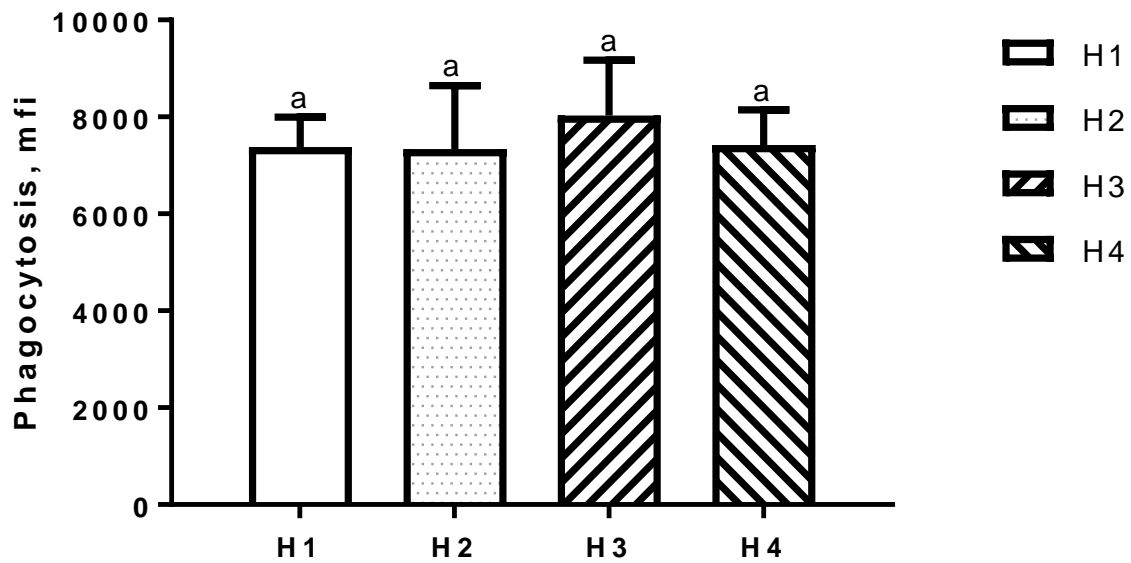


Fig. S1. Phagocytosis in different subpopulation of oyster hemocytes. Mfi – mean fluorescence intensity of phagocytosed fluorescent beads per 10⁴ cells. Different letters indicate values that are significantly different from each other (P<0.05). N=4-5.

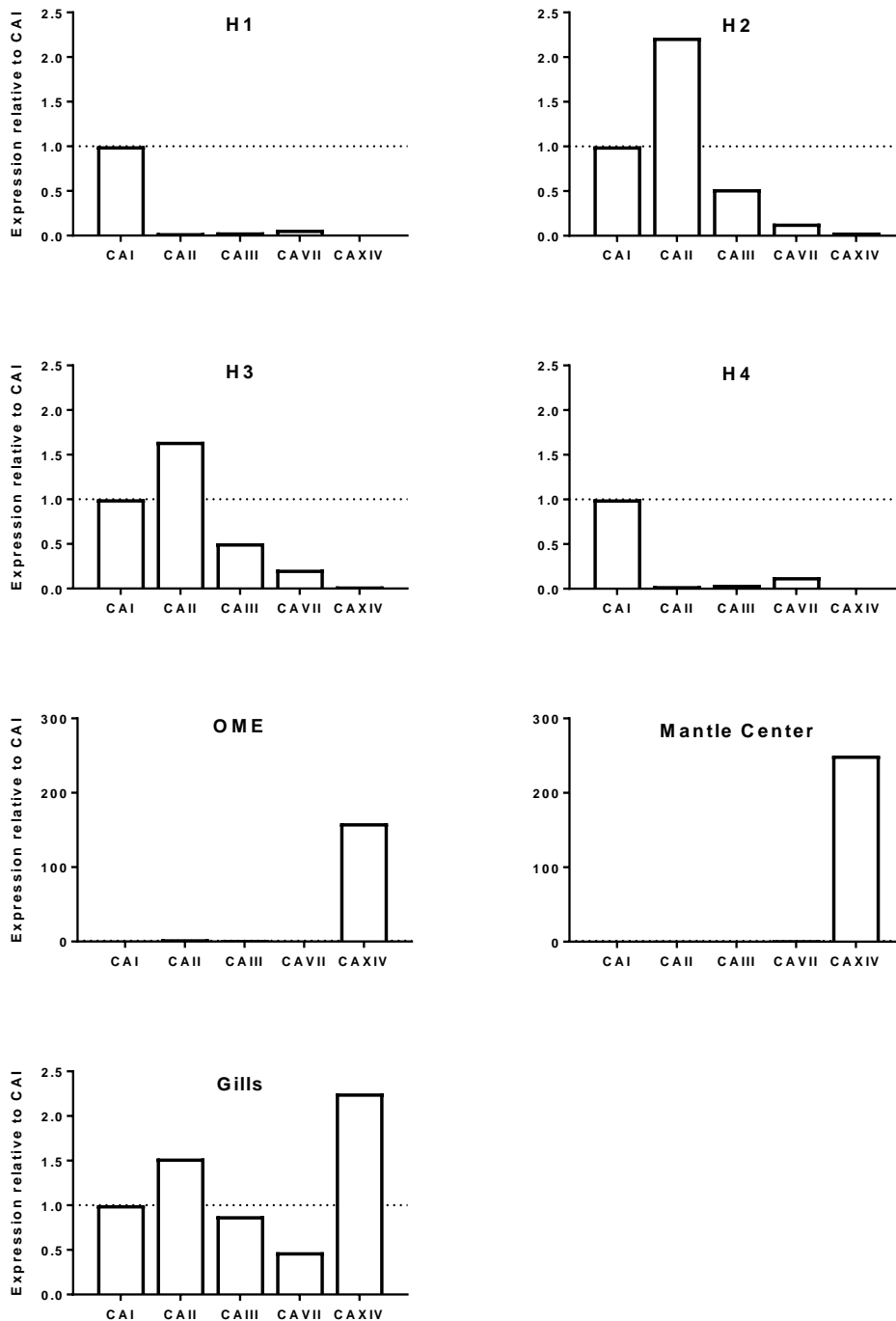


Fig. S2. mRNA expression profiles of different CA isoforms in the studied tissues and hemocyte fractions of *C. gigas*. Note similar CA profiles in the fractions H1 and H4, and the fractions H2 and H3, respectively. Hemocytes express soluble CAs (CAI, CAII, CAIII and CAVII), while the membrane-bound CA XIV is almost exclusively expressed in the mantle. The gills have CA expression profile similar to H2 and H3 hemocytes, except considerably higher levels of CA XIV expression in the gills. Expression of all CA isoforms is normalized to CAI levels.